ACS APPLIED MATERIALS & INTERFACES

Research Article

www.acsami.org

Electron Transport and Bulk-like Behavior of Wiedemann–Franz Law for Sub-7 nm-Thin Iridium Films on Silkworm Silk

Huan Lin,[†,‡,∥] Shen Xu,[‡,∥] Yu-Qing Zhang,*[,§] and Xinwei Wang*[,‡]

[†]School of Environmental and Municipal Engineering, Qingdao Technological University, Qingdao, Shandong 266033, People's Republic of China

[‡]2010 Black Engineering Building, Department of Mechanical Engineering, Iowa State University, Ames, Iowa 50011, United States

[§]Silk Biotechnology Key Laboratory of Suzhou City, School of Biology and Basic Medical Sciences, Soochow University, Suzhou 215123, People's Republic of China

ABSTRACT: For ultrathin metallic films, either supported or free-standing, the inside nanocrystalline nature significantly reduces the electron and thermal transport. Quantum mechanical reflection of electrons at the grain boundary reduces the electrical conductivity further than the thermal conductivity, leading to a Lorenz number in the order of 7.0×10^{-8} W Ω K^{-2}, much higher than that of the bulk counterpart. We report on a finding that for ultrathin (0.6–6.3 nm) iridium films coated on degummed silkworm silk fibroin, the electron transport is around 100–200% higher than that of the same film on glass fiber, even though the grain size of Ir film on silkworm silk is smaller than that on glass fiber. At the same time, the thermal conductivity of the Ir film is smaller or close to that of the film on glass fiber. Its Lorenz number is found close to that of bulk crystalline Ir despite the nanocrystalline structure in the Ir films. This is similar to the behavior of metallic glasses. Our study of gold films on silkworm silk reveals the same trend of change as compared to that on glass fiber. Electron hopping and tunneling in silkworm silk is speculated to be responsible for the observed electron transport. The finding points out that silk could provide a better substrate for flexible electronics with significantly faster electron transport.

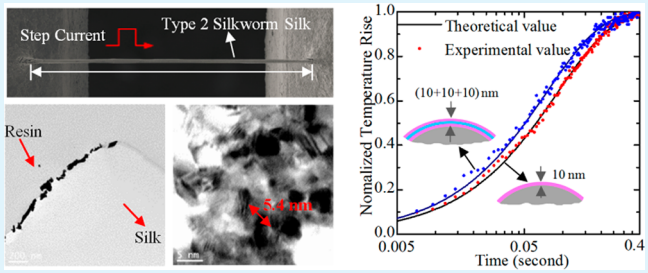

KEYWORDS: *silkworm silk, iridium film, gold film, electron transport, thermal conductivity, Lorenz number*

1. INTRODUCTION

When the grain/characteristic size of nanocrystalline metallic films is at the same level, or smaller than that of electron mean free path, the existence of grain boundary could strongly impede electron transport by quantum mechanical grain boundary electron reflection.[1−5] At the same time, because of the electron–phonon energy coupling at grain boundaries, the energy of the reflected electrons can be transferred across the grain boundary via electron–phonon scattering. The direct result is a significantly reduced electrical conductivity with a less reduced thermal conductivity.[6] The work by Yoneoka et al.[7] showed that a 7.3 nm free-standing Pt film has a significantly reduced electrical conductivity (77.8% reduction) and thermal conductivity (66.3% reduction). As a result, the Lorenz number (3.82×10^{-8} W Ω K^{-2}) becomes much higher than the bulk's value of 2.51×10^{-8} W Ω K^{-2}. In the work by Zhang et al.,[8,9] even higher Lorenz numbers have been found for 21–37 and 53 nm polycrystalline Au films: 7.0×10^{-8} and 5.0×10^{-8} W Ω K^{-2}. Our recent study[10] revealed significantly reduced electrical (93.7% reduction) and thermal (80.5% reduction) conductivities for a 6.4 nm gold (Au) film coated on a glass fiber. The film's Lorenz number was found almost 3 times the bulk's value. Such conclusion also holds for samples as thin as 0.6 nm as reported in our work[6] for iridium (Ir) on microscale glass fibers. Its electrical and thermal conductivities are only about 18% and 50% of that of bulk crystalline Ir. Its Lorenz number is also very high: 7.08×10^{-8} W Ω K^{-2}. The nanometer-thin films reported in the above work usually have nanocrystalline structure, which consists of many nanosize grains. When the grain size is very small (close to atomic level), the material will show an amorphous structure, as the case with metallic glass, and the situation becomes different. At 300 K, the electrical and thermal conductivities of metallic glasses are about (4.4–14.2) $\times 10^5$ Ω^{-1} m^{-1}[11−14] and 3.5–10.6 W m^{-1} K^{-1}.[11−17] These metallic glasses usually are alloys, like $Pd_{40}Ni_{40-x}Cu_xP_2$ and $Zr_{55}Al_{10}Ni_5Cu_{30}$. Mizoguchi et al. measured the Lorenz numbers in metallic glasses as $(2.2–3.2) \times 10^{-8}$ W Ω K^{-2} at 273 K. These numbers are very close to the theoretical value of 2.44×10^{-8} W Ω K^{-2} of bulk metal.[14]

In the past, Singh et al.[18] have conducted research on gold–spider silk conjugation and found the gold films can retain excellent electron transport. They attributed the electronic conduction in the spider silk fibers to electron tunneling and/or hopping. Eden et al.[19] found that amine-functionalized carbon nanotubes have strong affinity to spider silk. The coated silk fibers have an electrical conductivity that is strongly affected by

Received: March 27, 2014
Accepted: July 2, 2014
Published: July 2, 2014

strain and humidity. Their results revealed that the charge carrier transport is primarily sustained by charge hopping from tube to tube. Eden et al.[20] showed that sputtered gold film had very strong adherence to spider silks. This feature makes gold-coated spider silk a good candidate as excellent flexible connectors, especially at low temperatures.

In this work, we report on an intriguing work of sputtering coated Ir films (0.6−6.4 nm thickness) on silkworm silk to demonstrate that the electron transport is significantly higher than that in Ir films coated on glass fibers, although the grain size is smaller. Our detailed study on the thermal conductivity reveals it is either close to or smaller than that of the films on glass fiber. Its Lorenz number is found to be close to that of bulk crystalline structure, similar to the behavior of metallic glasses.

2. NANOCRYSTALLINE Ir ON SILKWORM SILK

Because of its unique mechanical strength and flexibility, silkworm silk has been used for thousands of years in textile fabrication.[21,22] In recent years, more work has been done to apply silkworm silk in biomedical and biotechnological engineering.[22−25] When used as a suture, the sericin needs to be removed from the silk fibroin fibers.[26] In this work, we focus on nanocrystalline metallic films on degummed single fiber of fibroin. Two degumming methods are used to process the silkworm silks used in this work. The degumming methods are briefed in section 5.1.

In this work, the Ir films on silk are grown using a sputtering coating machine (Quorum Q150T S). During Ir film deposition, the Ir atoms are uniformly deposited in space. The thickest region should be on top of the silkworm silk, and the local thickness is designated as δ_{max}. δ_{max} is monitored during deposition using a quartz crystal balance. The accuracy of measurement is verified by an atomic force microscope. Because of the circular shape of the silk, the Ir film thickness (δ_θ) varies on the silk surface as $\delta_\theta = \delta_{max} \cos \theta$ (θ: angle from the vertical direction). The average thickness of the film is calculated as $\delta_{ave} = 2\delta_{max}/\pi$.

We characterize the structure of the nanofilms by using a scanning electron microscope (SEM), X-ray diffraction (XRD), and transmission electron microscope (TEM). Details for these characterizations are listed in section 5.2. Figure 1a shows one of the silkworm silk samples with Ir coated from the top. It can be seen that the sericin removing process has been successful, and no sericin is observed on the fibroin surface. The XRD patterns of (δ_{ave}) 0.6, 1.3, 3.2, and 6.4 nm Ir nanofilms coated on silkworm silk are shown in Figure 1b. It is clear that when the film is very thin ($\delta_{ave} \leq 3.2$ nm), there is no visible peak. However, when the film becomes thicker, like 6.4 nm, the peak starts to emerge around 40.5°, revealing some crystalline structure in the film. We realize that XRD is not sufficient to reveal the structure. Therefore, the film structure is also studied by using a high-resolution TEM as shown in Figures 1c,f and 2. Figure 2c shows the electron diffraction pattern of the Ir film. The bright spots in the diffraction pattern clearly substantiate the existence of nanocrystals. Figure 2d shows a high-resolution TEM image of (δ_{max}) 20 nm Ir films coated on silkworm silk (Type 2). Evident nanocrystalline structure is observed under TEM, although such structure is barely revealed by the XRD study. On the basis of the lattice orientation variation shown in Figure 2d, the nanograin size is estimated to be around 5.4 nm, as marked in the figure. The stripe groups are multidirectional,

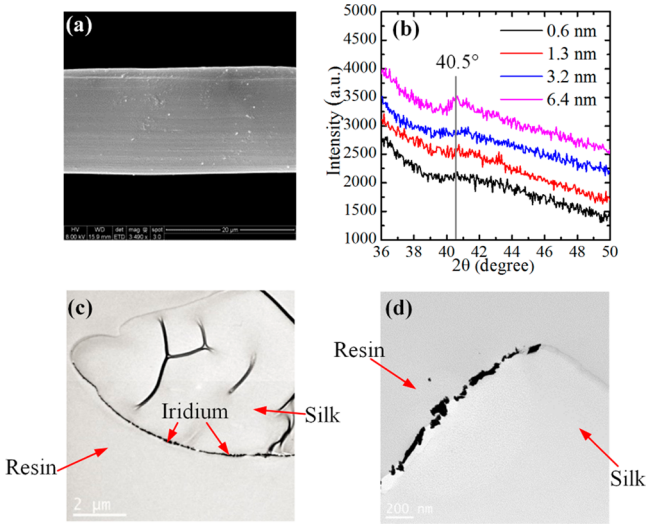

Figure 1. (a) SEM image of 6.4 nm-thick Ir coated on silkworm silk. (b) XRD patterns of Ir films coated on silkworm silk. For the film of 6.4 nm thick, a small peak appears at 40.5°, indicating the formation of crystalline structures. (c and d) Low-magnified TEM images of Ir film coated on silkworm silk studied in this work.

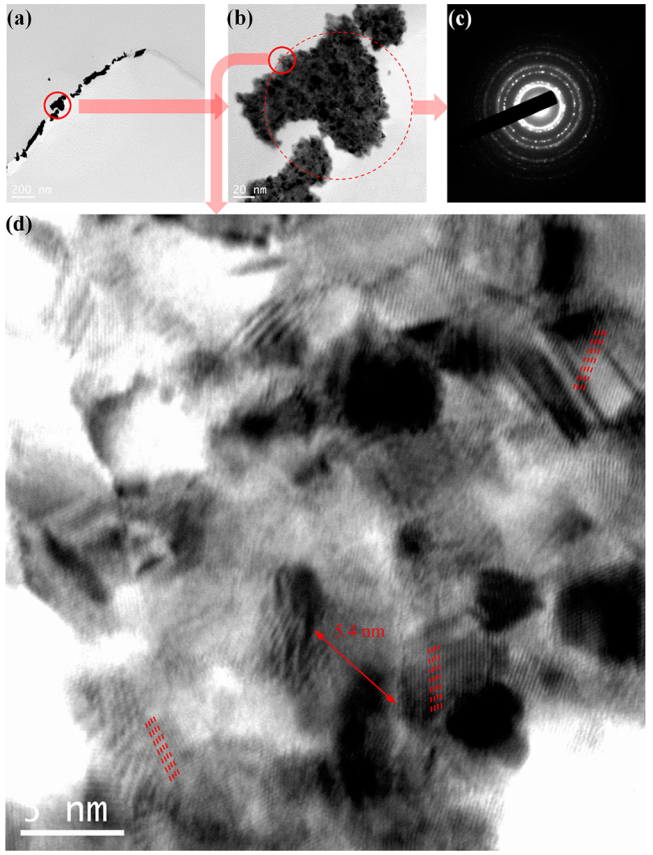

Figure 2. (a) TEM images of Ir film coated on silkworm silk under low magnification. (b) The magnified area from the red circle in (a). (c) The diffraction pattern for the dashed circle area in (b). The spots in the diffraction pattern clearly substantiate the existence of nanocrystals. (d) The high-resolution TEM image for the solid circle area in (b). The red dashed lines show the lattice orientation. The multiple orientations of strip groups in the image indicate the existence of nanocrystals.

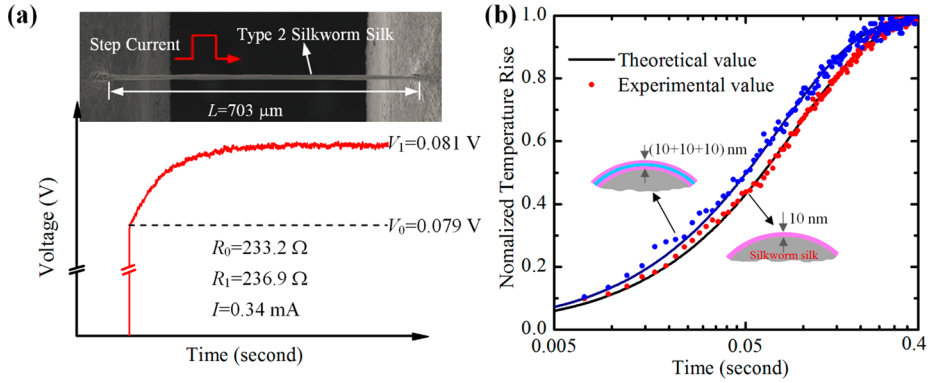

Figure 3. (a) The iridium coated silkworm silk connected between two electrodes and the measured voltage evolution for the sample. (b) Comparison between the theoretical fitting and experimental data for the normalized temperature rise for silkworm silk coated with Ir. The dots are experimental data of silkworm silk coated with three Ir layers (blue) and with single Ir layer (red), respectively. The upper and lower solid lines are theoretical fittings of silkworm silk coated with three Ir layers and single Ir layer. The normalized temperature rise of the sample with three Ir layers goes up faster than that with single Ir layer, meaning the effective thermal diffusivity of the silkworm silk with three Ir layers is bigger than that with a single Ir layer.

which means the Ir crystallographic orientation is different in each nanograin.

3. ELECTRON TRANSPORT AND BULK-LIKE WIEDEMANN–FRANZ LAW

A differential technology is applied to measure the thermal diffusivity/conductivity of Ir films. In this method, the silkworm silk is used as the base material to support the ultrathin Ir film. First, a Ir layer of thickness δ_1 is coated on the silk. The sample's effective thermal diffusivity (in the axial direction) is measured ($\alpha_{\text{eff},1}$). A second Ir layer of thickness δ_2 then is grown on the first Ir layer. The thermal diffusivity of this sample is measured as $\alpha_{\text{eff},2}$. In fact, the second Ir layer will give an increment in thermal diffusivity as $\Delta\alpha_{\text{eff}} = \alpha_{\text{eff},1} - \alpha_{\text{eff},2}$. This thermal diffusivity increment can be used to evaluate the thermal transport in the Ir layer.

In our work, the transient electro-thermal (TET) technique is used to measure the thermal diffusivity of Ir-coated silk. In TET measurement, the sample needs to be electrically conductive. The first Ir film is grown for such purpose. Theoretically, only one second Ir layer (δ_2 thickness) will be sufficient for electrical and thermal transport study in it. To suppress the experimental uncertainty/error, especially for ultrathin films, we repeat the process of adding a Ir layer of thickness δ_2 and measuring its thermal diffusivity $\alpha_{\text{eff},n}$. The relationship between $\alpha_{\text{eff},n}$ and the number (n) of the Ir layer (δ_2 thickness) is used for data processing. This treatment works nicely to improve the measurement accuracy. Because the deposited film layers (δ_2) have the same deposition condition and thickness, they have the same electrical and thermal conductivities and ρc_p.

The TET technique[27] is used for thermal characterization of Ir-coated silk. Details of this technique can be found in our previous work. A suspended sample used in TET characterization is shown in Figure 3a. Figure 3b demonstrates that after adding two 6.4 nm-thick Ir films, the thermal response of the sample to the step-current heating shows an appreciable difference that can be used to evaluate the thermal transport in the ultrathin Ir film. Details of this technique are given in section 5.3.

3.1. Electron Transport in Ir Film. The electrical resistance of the Ir film is related to the coating's electrical conductivity (σ) parameters as[6]

$$R_{\text{total}} = \frac{L}{A\cdot\sigma} = \frac{L}{D\cdot n\cdot\delta_{\max}\cdot\sigma} \tag{1}$$

The electrical conductivity σ for each δ_2 layer is considered to be the same, because all Ir layers have the same thickness. After three TET experiments, three groups data of (R_{total}^{-1}, n) can be obtained. Figure 4c is for the linear fitting of electrical conductance against the number of Ir layers (δ_{ave} = 6.4 nm) on top of a silkworm silk. The good linear relationship between R^{-1} and the number of layers indicates that each Ir layer has the same thickness and electrical conductivity. The fitted slope is 1.57×10^{-3} Ω^{-1}, and the electrical conductivity of the Ir film is calculated as 9.27×10^6 Ω^{-1} m^{-1}. This value is much larger than σ of 6.4 nm Ir layer deposited on glass fiber 3.23×10^6 Ω^{-1} m^{-1}.[6] For the Ir films coated on glass fiber, exactly the same deposition technique and condition were used. It means that ultrathin metallic films on silkworm silk provide an excellent platform for electrical connections that are preferred in flexible electronics.

The electrical conductivities of Ir films on silkworm silk and glass fibers both are much smaller than that of bulk Ir (σ_0), 19.68×10^6 Ω^{-1} m^{-1} at 300 K. The σ of Ir film on the glass fiber has a significant reduction of 83.6% from the bulk's value. For the Ir film on the silkworm silk, this reduction is only about 52.9%. Here, the Mayadas–Shatzkes (MS) model[28,29] is used to interpret the observed significant reduction in electron transport. In the MS model, σ_f/σ_0 is approximated by[30]

$$\frac{\sigma_f}{\sigma_0} = \left[1 + \frac{3(1-p)}{8k_0} + \frac{7}{5}\alpha\right]^{-1} \tag{2}$$

This equation has an error less than 9% for $\alpha < 10$ and $k_0 > 0.1$. $\alpha = l_0R/d(1-R)$, $k_0 = \delta_{\text{ave}}/l_0$, and σ_f and σ_0 are film and bulk electrical conductivities. l_0 is electron mean free path, d is the average grain size, R is the electron reflection coefficient at grain boundaries, p is the specular reflection parameter of electrons at film surfaces, and δ_{ave} is the average film thickness. This model is for films composed of grains that are in a "columnar" fashion normal to the film plane. The applicability of this equation to our sample has been fully justified in our previous work.[6] p can

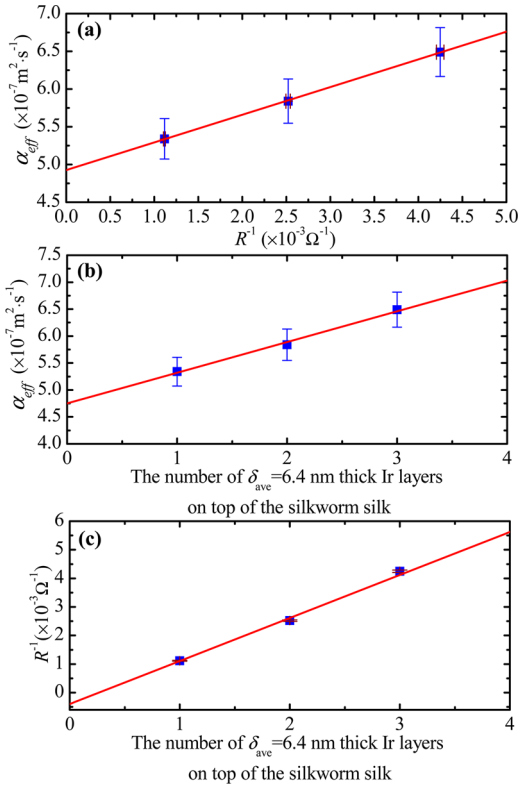

Figure 4. Data processing for determining the Lorenz number, thermal diffusivity, and electrical conductivity of the 6.4 nm Ir film on a silkworm silk of 703 μm length. (a) Variation of the effective thermal diffusivity of Ir-coated silkworm silk against the electrical conductance for 6.4 nm-thick Ir layers coated on the silkworm silk. The solid line is linear fitting of the three experimental data points. (b) Linear fitting of effective thermal diffusivity change with the number of Ir layers on top of the same silkworm silk sample shown in Figure 3a. (c) Linear fitting of electrical conductance change with the number of Ir layers on top of the silkworm silk. Solid lines are linear fittings of the experimental data. The error bars in measuring Lorenz number, electrical, and thermal conductivities are shown in the figure.

take "1" because σ changes little with the film thickness in our work. σ_0 is calculated from this relation: $L_{Lorenz} = k_c/\sigma T$. The Lorenz number of bulk Ir is 2.49×10^{-8} W Ω K^{-2} (273–373 K).[31] The Fermi energy (E_F) of Ir is 0.761 Ry,[32] and its Fermi velocity is 1.91×10^6 m s^{-1}. Because our experimental temperature is much lower than the Debye temperature and Fermi temperature, we can use $C = \gamma T$ (γ = 3.1 mJ mol^{-1} K^{-2})[31] for the electron's specific heat. Based on $k = Cv_F l_0/3$, l_0 is calculated as 2.04 nm.

For the 6.4 nm-thick Ir film discussed here, the grain size is about 5.4 nm as shown in Figure 2d. On the basis of the measured electrical conductivity, R is fitted to be 0.66. In comparison, R is determined as 0.93 for the same thickness Ir film on glass fiber.[6] The much smaller reflection coefficient for the Ir film on silkworm silk fibroin indicates that at grain boundaries, electrons have a greater chance to pass. We speculate this reduced grain boundary reflection is attributed to the electron hopping and tunneling in the adjacent fibroin that supports the Ir film.

3.2. Lorenz Number Evaluation. The measured α_{eff} reflects combined effects from both silk and the Ir coating as[27] $\alpha_{eff} = \alpha_w + L_{Lorenz}TL/(RA_w\rho c_p)$, where A_w is the cross-sectional area of silk. α_w is the real thermal diffusivity that still includes the effect of radiation. T and R are the sample's average temperature and electrical resistance during measurement. ρ and c_p are the sample's effective density and specific heat. This relation indicates that α_{eff} changes with R^{-1} linearly with a slope of $L_{Lorenz}TL/(A_w\rho c_p)$. Figure 4a shows the change of α_{eff} against R^{-1}. Our linear fitting yields a slope of 3.68×10^{-5} m^2 s^{-1} Ω (Figure 4a). In our TET measurements, the electrical current is controlled (160–340 μA) to give a moderate temperature rise around 7 K. An average temperature of 300 K is used in the Lorenz number calculation. Finally, the Lorenz number of 6.4 nm-thick Ir film is determined as 2.62×10^{-8} W Ω K^{-2}.

For bulk Ir, its Lorenz number is 2.49×10^{-8} W Ω K^{-2}[31] ($L_{Lorenz} = k_c/\sigma T$). Our measured Lorenz number 2.62×10^{-8} W Ω K^{-2} for the Ir film is very close to the bulk value (~5% difference). This demonstrates that the nanofilm structure deposited on silkworm silk has the same reduction effect in electron transport and thermal energy transport. Our previous work found the Lorenz numbers of 6.4 nm Ir and Au film coated on glass fiber are 6.15×10^{-8} W Ω K^{-2}[6] and 7.44×10^{-8} W Ω K^{-2},[10] respectively. Zhang et al.[8,9] have found that the Lorenz number of 21–37 and 53 nm polycrystalline Au films is around 7.0×10^{-8} and 5.0×10^{-8} W Ω K^{-2}. Zhang et al.[8,33,34] also reported that the Lorenz number of Pt nanofilms (15, 28, and 48 nm thickness) is also several times the bulk's value. These reported large values of the Lorenz number result from the grain boundary scattering, which imposes greater influence on the charge transport than heat conduction. For metallic glasses, their thermal conductivity (≤10.6 W m^{-1} K^{-1}) and electrical conductivity (≤14.2×10^5 Ω^{-1} m^{-1}) are much smaller than that of Ir film on silkworm silk. Their Lorenz number is around 1.57×10^{-8} to 2.64×10^{-8} W Ω K^{-2}. Although our material is nanocrystalline material, like metallic glasses, they have a Lorenz number close to that of the bulk counterpart. It means that the inside nanocrystalline/amorphous structure (random structure) did not alter the Lorenz number much. They have the same rate in reducing electron and thermal conduction.

3.3. Thermal Conductivity of the Ir Nanofilm. The measured α_{eff} can also be written as[6]

$$\alpha_{eff} = \alpha_w + \frac{4 \cdot n \cdot \delta_{max}}{\pi D(\rho c_p)_w}[k_c - \alpha_w(\rho c_p)_c] \quad (3)$$

where k is thermal conductivity, the subscript "c" refers to Ir layers, and "w" is for the silk. For silk and Ir, their ρc_p takes values of 1.36×10^6 J m^{-3} K^{-1}[35] and 2.49×10^6 J m^{-3} K^{-1}.[36] Equation 3 tells that α_{eff} changes with n linearly with a slope of $4\delta_{max}[k_c - \alpha_w(\rho c_p)_c]/\pi D(\rho c_p)_w$. Figure 4b shows the variation of α_{eff} against n. On the basis of linear fitting, the slope is found as 5.75×10^{-8} m^2 s^{-1}. The thermal conductivity of the Ir layer is then determined as 73.9 W m^{-1} K^{-1}. Note this value is larger than that of Ir deposited on glass fiber (66.1 W m^{-1} K^{-1}), but still much smaller than the k of bulk Ir (147 W m^{-1} K^{-1}) at 300 K. We believe the very small grains in the Ir films gives rise to strong electron grain boundary scattering, thereby greatly reducing the thermal conductivity.

3.4. Study of Ultrathin Films and Effect of Film Thickness. We characterized the electron and thermal transport in Ir films on Type 2 silkworm silk. The Ir films have an average thickness of 0.6, 1.3, 3.2, and 6.4 nm (corresponding to δ_{max} = 1, 2, 5, and 10 nm). The results are shown in Figure 5a–c. It should be pointed out that the

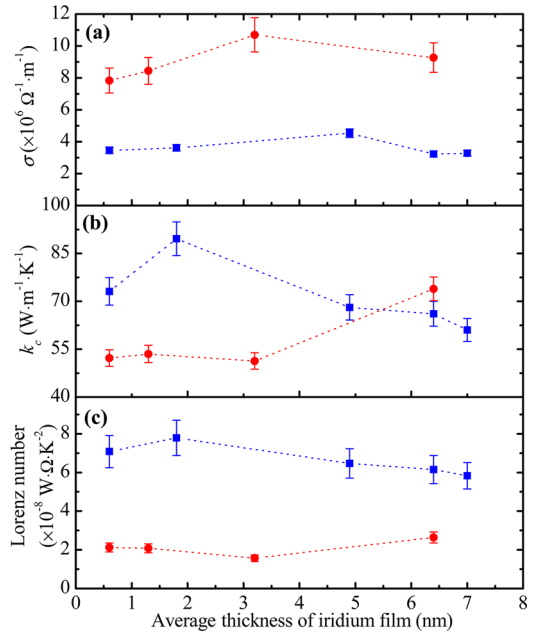

Figure 5. (a) δ_{ave}-dependent electrical conductivity of Ir films. (b) δ_{ave}-dependent thermal conductivity of Ir films. (c) Lorenz number variation against average thickness of Ir films. The data for Ir films coated on a glass fiber are also shown for comparison purpose. The blue squares are for films coated on glass fiber, and red dots are for films coated on silkworm silk.

measurement method for the 3.2 nm Ir coating is similar to that of the 6.4 nm-thick Ir coating. For very thin films (e.g., 0.6 nm), the experiment is revised because ultrathin Ir films are not electrically stable, making it hard to conduct the TET experiment. For such films, first, we coat an Ir layer of δ_{ave} = 3.2 nm on the silk as the base layer, and measure the sample's α_{eff}. After that, an ultrathin Ir film (δ_{ave} = 0.6 or 1.3 nm) is added, and the corresponding α_{eff} is measured for several rounds. α_{eff} is related to R as $\alpha_{eff} = \alpha + L_{1,Lorenz}TL\cdot R_1^{-1}/(A_w\rho c_p) + L_{2,Lorenz}TL\cdot R_{2,n}^{-1}/(A_w\rho c_p)$, where R_1 is for the base Ir layer and R_{2n} (n = 1−5) is for the n layers of Ir film. Subscripts "1" and "2" are for the base layer and ultrathin Ir layer. Using a similar method to determine the Lorenz number of the δ_{ave} = 6.4 nm Ir layer, we determine the Lorenz number of δ_{ave} = 0.6 and 1.3 nm Ir layer as 2.12×10^{-8} and 2.06×10^{-8} W Ω K^{-2}, respectively.

α_{eff} is also related to the thermal conductivity of the Ir layer as

$$\alpha_{eff} = \alpha_w + \frac{1}{(\rho c_p)_w}\frac{4\delta_{1,max}}{\pi D}[k_1 - \alpha_w(\rho c_p)_c] + \frac{1}{(\rho c_p)_w}\frac{4n\cdot\delta_{2,max}}{\pi D}[k_2 - \alpha_w(\rho c_p)_c] \quad (4)$$

Subscripts "1" and "2" are for the base layer and one individual ultrathin Ir layer. By linear fitting of the change of α_{eff} and R against n, we can determine the thermal conductivity and electrical conductivity of ultrathin Ir films.

Figure 5a−c also shows the comparisons between films coated on glass fiber and silkworm silk for electrical conductivity, thermal conductivity, and Lorenz number. The blue squares are for films coated on glass fiber, and red dots are for films coated on silkworm silk. For Ir films on silkworm silk, the measured thermal and electrical conductivities have an uncertainty less than 10% and 5%, respectively. The Lorenz number has an uncertainty less than 11%. The electrical conductivity has a substantial increase (∼37%) when the thickness of Ir films on silkworm silk increases from 0.6 to 3.2 nm. On the other hand, the electrical conductivity stays pretty much constant for the Ir films on glass fiber against the film thickness. It is evident that the electrical conductivity of films coated on silkworm silk is almost 2-fold that of films coated on glass fiber. This substantial increase in electron transport is attributed to the unique structure of silkworm silks. Like the behavior of electronic conduction in the spider silk fibers,[18,19] the electron tunneling and hopping in silkworm silk can enhance the electronic conduction. When the Ir is thin (<5 nm), its thermal conductivity is smaller than thermal conductivity of films coated on glass fiber. The possible reason is the grain size of Ir film coated on silkworm silk (5.4 nm) is smaller than that on glass fiber (8.8 nm), which gives stronger grain boundary phonon scattering. The larger k and smaller σ make the Lorenz number less than that of the film on glass fiber and close to that of bulk crystalline structure. This is like the behavior of metallic glass.

We have conducted separate experiments to check the electrical contact resistance at the sample/base contact. For Ir-coated silkworm silk, the silver paste significantly enhances the local electrical contact. The contact resistance is found around 10 Ω or less.

3.5. Discussion about Ultrathin Gold Films on Silkworm Silk. To have a better understanding of electron and thermal transport in thin films, we also did the measurement of 12.8 nm-thick Au films deposited on Type 1 silkworm silk fiber, in anticipation to compare with that in Ir films. A 736 μm long silkworm silk is coated with 12.8 nm Au layer by layer using a sputtering machine (Denton Vacuum Desk V-Standard). The Au film is found having σ, k, and Lorenz number as 4.90×10^6 Ω^{-1} m^{-1}, 31.8 W m^{-1} K^{-1}, and 2.08×10^{-8} W· Ω K^{-2}.

In our previous work,[10] the σ and k of 6.4 nm-thick Au on a glass fiber are 2.71×10^6 Ω^{-1} m^{-1} and 61.9 W m^{-1} K^{-1}. These values have a great reduction from the bulk's value: 93.7% for σ and 80.5% for k. Its Lorenz number is 7.44×10^{-8} W Ω K^{-2}, almost 3 times the bulk's value. For Au film on silkworm silk, its rough surface and large grain size of gold during sputtering make it impossible to deposit 6.4 nm-thick gold on silkworm silk to reproduce the same scenario as that on glass fiber. It is clear that Au film on silkworm silk has a smaller k and higher σ than that on the glass fiber. The resulting difference is not induced by the Au film thickness because k and σ have different trends of change. Rather it is induced by the substrate: silkworm silk. The thermal conductivity of Au film on silkworm silk is almost one-half of that on glass fiber. On the other hand, the electrical conductivity of Au film on silkworm silk is almost twice that on glass fiber. For Ir films, the thermal conductivity decrease is not significant. The thermal conductivity of 6.4 nm Ir film coated on silkworm silk is only a little higher than that on glass fiber. The difference in thermal conductivity reduction may be attributed to the film structural difference: the Ir film has a finer structure than the Au film.

4. CONCLUSION

We have investigated the electron and thermal transport in ultrathin Ir films coated on degummed silkworm silk fibroin. The Ir film thickness was varied from 0.6 nm (∼3 atomic layers) to 6.4 nm. The electrical conductivity of the Ir film is around (7.8−10.7) × 10^6 Ω^{-1} m^{-1}, about a 100−200% increase

from that of the same film on glass fiber, even though the grain size of Ir film on silkworm silk is smaller than that on glass fiber. The thermal conductivity of Ir films on silkworm silk is about 52.2−73.9 W m^{-1} K^{-1}, close to that of the film on glass fiber when the film is thick. For thin Ir films on silkworm silk (<5 nm), its thermal conductivity can be much smaller than that on glass fiber. The Lorenz number is found significantly less than that of the film on glass fiber and close to that of bulk crystalline structure. This behavior of the Ir film, despite its nanocrystalline structure, is like the behavior of metallic glasses. We feel the substantial increase of electron transport is attributed to the unique structure of silkworm silks. The electron tunneling and hopping in silkworm silk could enhance the electron conduction. Our further work on Au films deposited on silkworm silk showed the similar trend in comparison with that on glass fiber: great σ increase (~80%), k decrease, and a Lorenz number close to the bulk's value.

5. METHODS AND EXPERIMENTS

5.1. Sample Preparation. For Type 1 silk fibroin fiber, it was degummed using a 0.2% (w/v) neutral soap solution, followed by heating at 30 min at 100 °C, deionized water washing, and air drying. To prepare Type 2 silk fibroin, clean cocoon shells were degummed by a 0.5% (w/v) Na_2CO_3 solution at 98 °C. The samples then were rinsed with deionized water, followed by air drying at 105 °C for 2 h. In this work, Type 2 silk fibroin fibers are used for the study of Ir films, and Type 1 silk fibroin fiber is used for Au film. Details of the degumming process are given in our previous work.[35]

5.2. Structure Characterization. In SEM characterization, the same sample used in TET measurement is used here. The measurement is conducted at a high vacuum mode with a voltage of 8 kV. For XRD characterization, one silk filament is too small as compared to the XRD spot size, so a bunch of silk filaments are used. Those silk filaments are arranged to be parallel to each other and then to form a flat "film". This "film" is fixed on a glass substrate and coated with a 20 nm-thick Ir film (δ_{max} = 20 nm). The coating method is a little different among 0.6, 1.3, 3.2, and 6.4 nm-thick Ir film samples (corresponding to δ_{max} = 1, 2, 5, and 10 nm). For example, the 0.6 nm-thick Ir film on silkworm silk used for XRD characterization is composed of 20 layers of Ir film with δ_{max} = 1 nm. The XRD (Siemens D500) is equipped with a copper X-ray tube. The scanning angle for our samples is from 36° to 50°.

TEM studies are carried out by using a JEOL 1200EX TEM with a 1.4 Å resolution. For sample preparation, a liquid resin is used with plasticizers and then mixed together with silkworm silks. This liquid mixture is poured in a mold and allowed to slowly polymerize at room temperature. After the solidification, this resin with fibers is sliced into thin pieces as samples for TEM study.

5.3. Effective Thermal Diffusivity Characterization. As illustrated in Figure 3a, the to-be-measured Ir-coated silkworm silk is connected between two aluminum electrodes using silver paste. To reduce the effect of air convection, the experiment is conducted in a vacuum chamber. During TET measurement, a square-wave DC current is passed through the sample. Figure 3a shows the voltage variation history for one of the measurements. After being coated with three layers of δ_{ave} = 6.4 nm Ir film on top of 703 μm long Type 2 silkworm silk, the resistance is 233.2 Ω. A current of 0.34 mA is used in this experiment. This leads to a moderate voltage increase as shown in the figure. Because the current is constant, the observed voltage increase from V_0 to V_1 is induced by the resistance increase of the sample. This small resistance increase is caused by the temperature rise of the sample, and is linearly proportional to the temperature rise because the temperature rise is moderate (detailed later). The normalized overall temperature rise T^*_{exp} of the sample can be calculated as $T^*_{exp} = (V_{sample} - V_0)/(V_1 - V_0)$. The theoretical nondimensional temperature rise T^* is related to the thermal diffusivity α and sample length L as

$$T^* = \frac{96}{\pi^4}\sum_{m=1}^{\infty}\frac{1-\exp[-(2m-1)^2\pi^2\alpha t/L^2]}{(2m-1)^4} \quad (5)$$

This equation is used to fit the experimental data to determine α. More details on how data are processed and fitted are given in our previous work.[6] The TET technique has been verified by measuring the thermal conductivity and diffusivity of various micro-/nanoscale wires. Usually, a sound accuracy as good as 5% can be achieved.[27,37−40]

We take the δ_{ave} = 6.4 nm Ir film as an example to describe the data processing. First, we coat one Type 2 silkworm silk (703 μm long) with one Ir layer and measure its α_{eff}. We then add another δ Ir layer and do the TET experiment again. Three times of TET experiments with the same silkworm silk coated with Ir layers have been conducted. Figure 3b shows the normalized temperature rise and the fitting result. It is clear that with three Ir layers, the normalized temperature rise of the sample reaches the steady state faster than that with a single Ir layer. This means indeed more Ir layers make α_{eff} higher. α_{eff} values of these two samples are determined at 6.49 × 10^{-7} and 5.34 × 10^{-7} m^2 s^{-1}.

AUTHOR INFORMATION

Corresponding Authors

*Tel.: +86 512 65880181. E-mail: sericult@suda.edu.cn.
*Tel.: (515) 294-8023. E-mail: xwang3@iastate.edu.

Author Contributions

‖These authors contributed equally.

Notes

The authors declare no competing financial interest.

ACKNOWLEDGMENTS

We are thankful for the great support of this work by the Army Research Office (W911NF-12-1-0272), Office of Naval Research (N000141210603), and National Science Foundation (CMMI-1264399). We are grateful to Christopher Reilly for his careful proofreading of the manuscript.

REFERENCES

(1) Fuchs, K. The Conductivity of Thin Metallic Films According to the Electron Theory of Metals. *Proc. Cambridge Philos. Soc.* **1938**, *34*, 100−108.

(2) Sondheimer, E. H. The Mean Free Path of Electrons in Metals. *Adv. Phys.* **1952**, *1*, 1−42.

(3) Soffer, S. B. Statistical Model for Size Effect in Electrical Conduction. *J. Appl. Phys.* **1967**, *38*, 1710−1715.

(4) Namba, Y. Resistivity and Temperature Coefficient of Thin Metal Films with Rough Surface. *Jpn. J. Appl. Phys.* **1970**, *9*, 1326−1329.

(5) Gurrum, S. R.; Joshi, Y. K.; King, W. P.; Ramakrishna, K. Numerical Simulation of Electron Transport through Constriction in a Metallic Thin Film. *IEEE Electron Device Lett.* **2004**, *25*, 696−698.

(6) Lin, H.; Xu, S.; Wang, X.; Mei, N. Thermal and Electrical Conduction in Ultra-thin Metallic Films: 7 nm down to Sub-nm Thickness. *Small* **2013**, *9*, 2585−2594.

(7) Yoneoka, S.; Lee, J.; Liger, M.; Yama, G.; Kodama, T.; Gunji, M.; Provine, J.; Howe, R. T.; Goodson, K. E.; Kennyt, T. W. Electrical and Thermal Conduction in Atomic Layer Deposition Nanobridges down to 7 nm Thickness. *Nano Lett.* **2012**, *12*, 683−686.

(8) Wang, H. D.; Liu, J. H.; Zhang, X.; Guo, Z. Y.; Takahashi, K. Experimental Study on the Influences of Grain Boundary Scattering on the Charge and Heat Transport in Gold and Platinum Nanofilms. *Heat Mass Transfer* **2011**, *47*, 893−898.

(9) Zhang, Q. G.; Cao, B. Y.; Zhang, X.; Fujii, M.; Takahashi, K. Influence of Grain Boundary Scattering on the Electrical and Thermal Conductivities of Polycrystalline Gold Nanofilms. *Phys. Rev. B* **2006**, *74*, 134109.

(10) Lin, H.; Xu, S.; Li, C.; Dong, H.; Wang, X. Thermal and Electrical Conduction in 6.4 nm Thin Gold Films. *Nanoscale* **2013**, *5*, 4652−4656.
(11) Harms, U.; Shen, T.; Schwarz, R. Thermal Conductivity of $Pd_{40}Ni_{40-x}Cu_xP_{20}$ Metallic Glasses. *Scr. Mater.* **2002**, *47*, 411−414.
(12) Yamasaki, M.; Kagao, S.; Kawamura, Y. Thermal Diffusivity and Conductivity of $Zr_{55}Al_{10}Ni_5Cu_{30}$ Bulk Metallic Glass. *Scr. Mater.* **2005**, *53*, 63−67.
(13) Umetsu, R. Y.; Tu, R.; Goto, T. Thermal and Electrical Transport Properties of Zr-based Bulk Metallic Glassy Alloys with High Glass-forming Ability. *Mater. Trans.* **2012**, *53*, 1721−1725.
(14) Mizoguchi, T.; Kudo, T.; Takayama, S. Lorenz Number in Metallic Glasses. *J. Phys., Colloq.* **1980**, *41*, C8-501−C8-502.
(15) Choy, C.; Tong, K.; Wong, H.; Leung, W. Thermal Conductivity of Amorphous Alloys above RoomTemperature. *J. Appl. Phys.* **1991**, *70*, 4919−4925.
(16) Louzguine-Luzgin, D. V.; Saito, T.; Saida, J.; Inoue, A. Thermal Conductivity of Metallic Glassy Alloys and its Relationship to the Glass Forming Ability and the Observed Cooling Rates. *J. Mater. Res.* **2008**, *23*, 2283−2287.
(17) Choy, C.; Leung, W.; Ng, Y. Thermal Conductivity of Metallic Glasses. *J. Appl. Phys.* **1989**, *66*, 5335−5339.
(18) Singh, A.; Hede, S.; Sastry, M. Spider Silk as an Active Scaffold in the Assembly of Gold Nanoparticles and Application of the Gold−silk Bioconjugate in Vapor Sensing. *Small* **2007**, *3*, 466−473.
(19) Steven, E.; Saleh, W. R.; Lebedev, V.; Acquah, S. F.; Laukhin, V.; Alamo, R. G.; Brooks, J. S. Carbon Nanotubes on a Spider Silk Scaffold. *Nat. Commun.* **2013**, *4*, 2435.
(20) Steven, E.; Park, J. G.; Paravastu, A.; Lopes, E. B.; Brooks, J. S.; Englander, O.; Siegrist, T.; Kaner, P.; Alamo, R. G. Physical Characterization of Functionalized Spider Silk: Electronic and Sensing Properties. *Sci. Technol. Adv. Mater.* **2011**, *12*, 055002.
(21) Asakura, T.; Sugino, R.; Yao, J. M.; Takashima, H.; Kishore, R. Comparative Structure Analysis of Tyrosine and Valine Residues in Unprocessed Silk Fibroin (silk I) and in the Processed Silk Fiber (silk II) from Bombyx Mori using Solid-state C-13, N-15, and H-2 NMR. *Biochemistry* **2002**, *41*, 4415−4424.
(22) Hu, X.; Kaplan, D.; Cebe, P. Determining Beta-sheet Crystallinity in Fibrous Proteins by Thermal Analysis and Tnfrared Spectroscopy. *Macromolecules* **2006**, *39*, 6161−6170.
(23) Altman, G. H.; Diaz, F.; Jakuba, C.; Calabro, T.; Horan, R. L.; Chen, J. S.; Lu, H.; Richmond, J.; Kaplan, D. L. Silk-based Biomaterials. *Biomaterials* **2003**, *24*, 401−416.
(24) Foo, C. W. P.; Kaplan, D. L. Genetic Engineering of Fibrous Proteins: Spider Dragline Silk and Collagen. *Adv. Drug Delivery Rev.* **2002**, *54*, 1131−1143.
(25) Demura, M.; Asakura, T.; Kuroo, T. Immobilization of Biocatalysts with Bombyx-Mori Silk Fibroin by Several Kinds of Physical Treatment and Its Application to Glucose Sensors. *Biosensors* **1989**, *4*, 361−372.
(26) Altman, G. H.; Diaz, F.; Jakuba, C.; Calabro, T.; Horan, R. L.; Chen, J.; Lu, H.; Richmond, J.; Kaplan, D. L. Silk-based Biomaterials. *Biomaterials* **2003**, *24*, 401−416.
(27) Guo, J. Q.; Wang, X. W.; Wang, T. Thermal Characterization of Microscale Conductive and Nonconductive Wires using Transient Electrothermal Technique. *J. Appl. Phys.* **2007**, *101*, 063537.
(28) Mayadas, A. F.; Shatzkes, M. Electrical-resistivity Model for Polycrystalline Films - Case of Arbitrary Reflection at External Surfaces. *Phys. Rev. B* **1970**, *1*, 1382−1389.
(29) Mayadas, A. F.; Shatzkes, M.; Janak, J. F. Electrical Resistivity Model for Polycrystalline Films - Case of Specular Reflection at External Surfaces. *Appl. Phys. Lett.* **1969**, *14*, 345−347.
(30) Qiu, T. Q.; Tien, C. L. Size Effects on Nonequilibrium Laser-heating of Metal-films. *J. Heat Transfer* **1993**, *115*, 842−847.
(31) Kittel, C. *Introduction to Solid State Physics*, 5th ed.; Wiley: New York, 1976; xiv, 599 pp.
(32) Andersen, O. K. Mackinto.Ar. Fermi Surfaces and Effective Masses in Fcc Transition Metals. *Solid State Commun.* **1968**, *6*, 285−290.
(33) Zhang, X.; Xie, H. Q.; Fujii, M.; Ago, H.; Takahashi, K.; Ikuta, T.; Abe, H.; Shimizu, T. Thermal and Electrical Conductivity of a Suspended Platinum Nanofilm. *Appl. Phys. Lett.* **2005**, *86*, 171912.
(34) Zhang, X.; Zhang, Q. G.; Cao, B. Y.; Fujii, M.; Takahashi, K.; Ikuta, T. Experimental Studies on Thermal and Electrical Properties of Platinum Nanofilms. *Chin. Phys. Lett.* **2006**, *23*, 936−938.
(35) Liu, G.; Huang, X.; Wang, Y.; Zhang, Y.-Q.; Wang, X. Thermal Transport in Single Silkworm Silks and the Behavior under Stretching. *Soft Matter* **2012**, *8*, 9792−9799.
(36) Incropera, F. P. *Fundamentals of Heat and Mass Transfer*, 6th ed.; John Wiley: Hoboken, NJ, 2007; xxv, 997 pp.
(37) Feng, X.; Wang, X.; Chen, X.; Yue, Y. Thermo-physical Properties of Thin Films Composed of Anatase TiO2 Nanofibers. *Acta Mater.* **2011**, *59*, 1934−1944.
(38) Feng, X. H.; Huang, X. P.; Wang, X. W. Thermal Conductivity and Secondary Porosity of Single Anatase TiO2 Nanowire. *Nanotechnology* **2012**, *23*, 185701.
(39) Ma, Y. W.; Zhang, L. R.; Li, J. J.; Ni, H. T.; Li, M.; Zhang, J. L.; Feng, X. M.; Fan, Q. L.; Hu, Z.; Huang, W. Carbon-Nitrogen/Graphene Composite as Metal-free Electrocatalyst for the Oxygen Reduction Reaction. *Chin. Sci. Bull.* **2011**, *56*, 3583−3589.
(40) Guo, J. Q.; Wang, X. W.; Zhang, L. J.; Wang, T. Transient Thermal Characterization of Micro/submicroscale Polyacrylonitrile Wires. *Appl. Phys. A: Mater. Sci. Process.* **2007**, *89*, 153−156.